



OPEN ACCESS

Extensional flow of low-viscosity fluids in capillary bridges formed by pulsed surface acoustic wave jetting

To cite this article: P K Bhattacharjee *et al* 2011 *New J. Phys.* **13** 023005

View the [article online](#) for updates and enhancements.

You may also like

- [Predictions of criticality in inverted water columns](#)
Kezhao Bai, Zhi Yang, Zhuokun Hu et al.
- [Experimental investigations of liquid bridge rupture between a sphere and a spherical concave](#)
Congcong Huang, Zenghua Fan, Han Wang et al.
- [Simulation of capillary-driven kinetics with multi-phase-field and lattice Boltzmann method](#)
Raphael Schiedung, Marvin Tegeler, Dmitry Medvedev et al.

Extensional flow of low-viscosity fluids in capillary bridges formed by pulsed surface acoustic wave jetting

P K Bhattacharjee, A G McDonnell, R Prabhakar, L Y Yeo
and J Friend¹

MicroNanophysics Research Laboratory, Department of Mechanical and
Aerospace Engineering, Monash University, Melbourne, VIC 3800, Australia
and
Melbourne Centre for Nanofabrication, Melbourne, VIC 3800, Australia
E-mail: james.friend@monash.edu.au

New Journal of Physics **13** (2011) 023005 (14pp)

Received 22 July 2010

Published 1 February 2011

Online at <http://www.njp.org/>

doi:10.1088/1367-2630/13/2/023005

Abstract. Forming capillary bridges of low-viscosity ($\lesssim 10$ mPa s) fluids is difficult, making the study of their capillary-thinning behavior and the measurement of the fluid's extensional viscosity difficult as well. Current techniques require some time to form a liquid bridge from the stretching of a droplet. Rapidly stretching a liquid bridge using these methods can cause its breakup if the viscosity is too low. Stretching more slowly allows the bridge to thin and break up before a suitable bridge geometry can be established to provide reliable and accurate rheological data. Using a pulsed surface acoustic wave to eject a jet from a sessile droplet, a capillary bridge may be formed in about 7.5 ms, about seven times quicker than current methods. With this approach, capillary bridges may be formed from Newtonian and non-Newtonian fluids having much lower viscosities—water, 0.04% by weight solution of high-molecular-weight (7 MDa) polystyrene in dioctyl phthalate and 0.25% fibrinogen solution in demineralized water, for example. Details of the relatively simple system used to achieve these results are provided, as are experimental results indicating deviations from a Newtonian response by the low-viscosity non-Newtonian fluids used in our study.

¹ Author to whom any correspondence should be addressed.

Contents

1. Introduction	2
2. Experiment	4
3. Results	8
3.1. Benchmark solutions	8
3.2. Fibrinogen	11
4. Conclusions	13
Acknowledgment	13
References	13

1. Introduction

Many branches of science and engineering rely upon accurate and complete knowledge of the behavior of fluids. For hydrodynamically simple—*Newtonian*—fluids, this knowledge is usually obtained without much difficulty: a constant viscosity to go with a density and surface tension. But for arguably a majority of fluids, neither the behavior nor the measurement is so simple. Complex fluids, common in biology and engineering and as diverse as blood to adhesives, possess deformable microstructure that gives rise to at least one non-constant and perhaps time-dependent viscosity. Fortunately, elongational flows offer a strong irrotational deformation; within such fluids these flows are capable of aligning such microstructure, whether flexible polymer molecules, red blood cells or asymmetric rigid bodies, along the direction of the flow. The flow-induced alignment of flexible polymer molecules enables the study of properties that arise from the intrinsic connectivity of the molecular backbone and from peculiarities in the architecture of the molecule [1]. One can employ elongational flows to determine the properties of fluids from simple to complex, and in recent times the application of elongational flows to the study of the dynamics of complex fluids has become an area of significant research activity.

Creating and sustaining uniaxial elongational flows in the laboratory, however, has been challenging, and reliable rheometric techniques using elongational flows have only been developed in the past two decades. One such technique that is particularly relevant to this study is capillary breakup elongational rheometry (CaBER), using surface tension-driven necking of a liquid bridge to study the evolution of fluid microstructure under elongational deformation [2]. However, the technique is currently limited to fluids possessing modest to extremely large viscosities. A remarkable variety of low-viscosity fluids, including biological fluids and nano-particle suspensions, cannot be currently studied using CaBER. In the following, we demonstrate that microjets generated using surface acoustic waves (SAWs) [3] can be used to replicate the CaBER technique at much smaller length scales using fluids of lower viscosities outside the range of CaBER. Because the new approach works at a physical scale much smaller than is typical with CaBER, quantitative measurements of non-Newtonian behavior of low-viscosity fluids undergoing extensional flow can be made using much less fluid, only a few microliters. This new technique permits an improved characterization of low-viscosity fluids having a small but finite elastic component, and may provide insight into the mechanisms that lead to the finite time singularity that occurs when a liquid column necks down and breaks under the influence of surface tension [4]–[7] in the limit of low fluid viscosity. As we aim to focus

upon the concept and system rather than an in-depth study of non-Newtonian fluids whatever the viscosity, we will show the behavior of the system with Newtonian and non-Newtonian fluids, while only noting the deviation from typical Newtonian behavior in the latter case. Such deviations for very low-viscosity polymer solutions are reported here for the first time.

The CaBER technique allows the study of the dynamics of a fluid over a broad range of length scales, limited at the smaller end by the spatial resolution of the measurement instruments. With CaBER, a small volume of a fluid to be tested is placed in the gap formed between two parallel end-plates. By rapidly separating one of the two plates along a direction perpendicular to their faces, a liquid bridge is first formed. The motion of the end-plate is stopped when a predetermined separation between the plates is reached. The bridge then subsequently necks down and breaks under the influence of surface tension forces. The flow at the plane of the minimum neck radius is well approximated as a uniaxial extensional or stretching flow. Further, the time dependence of the approach to breakup of the minimum neck radius R_{neck} of the fluid strand under these conditions depends on the stress response of the fluid to an imposed extensional flow, and is well understood for Newtonian fluids, whereas in more complex non-Newtonian fluids, it is governed by the dynamics of the fluid microstructure. The central idea of the CaBER device is that the observed $R_{\text{neck}}(t)$ can be used to understand the behavior of complex fluids in extensional flows. An additional advantage of CaBER is the reliable location of the minimum (instantaneous) neck radius, $R_{\text{neck}}(t)$, at the mid-plane of the fluid column due to the confined geometry of the liquid bridge. This makes following the necking processes easier than other techniques like jet breakup [8] and drop pinchoff [9, 10] where the position of the neck varies in both time and space from one test to another.

For complex fluids, as the liquid bridge narrows and the length scale of the flow (ℓ) near the narrow neck region of the bridge decreases, non-Newtonian effects can be dramatically amplified as the Deborah number $De = \lambda V/\ell$ and the elasticity number $El = \eta_0 \lambda/\rho \ell^2$ both increase to values greater than unity. Here η_0 is the zero-shear-rate viscosity of the fluid, λ is the characteristic relaxation time of the viscoelastic fluid, V is the characteristic velocity of flow and ρ is the density of the fluid. At small length scales, the influence of inertia decreases with the Reynolds number $Re = \rho V \ell/\eta_0$ and the non-Newtonian effects become more conspicuous even for small values of η_0 and V .

Extending the CaBER technique with current technology to low-viscosity non-Newtonian fluids is prevented by the difficulty in forming liquid bridges of these fluids. A bridge is created in a CaBER system from a fluid drop by separating the two end-plates holding the drop. If the duration of this ‘opening time’ δt_0 exceeds the viscous time, $\tau_v = 14.1 \eta_0 R/\gamma$, where R is the radius of the droplet and γ is the surface tension coefficient of the fluid, the liquid thread can disintegrate even before the separation of the plates is completed. Additionally, inertio-capillary oscillations of the bridge that result from the abrupt halting of the end-plates in CaBER can disrupt the liquid bridge immediately after its formation if the viscosity is too low. The other problems associated with the use of the CaBER technique for extensional rheometric characterization of low-viscosity fluids are discussed in detail elsewhere [11].

Returning to the problem of bridge formation, we can estimate $\eta_{0,\text{min}}$, the minimum viscosity necessary for bridge formation, by equating plate separation and viscous times, i.e. $\delta t_0 = \tau_v$. Hence, $\eta_{0,\text{min}} \sim \delta t_0 \gamma/(14.1 R)$, and for a typical Newtonian fluid with $\gamma = 60 \times 10^{-3} \text{ N m}^{-1}$, and for values of $R = 3 \text{ mm}$ and $\delta t_0 = 50 \text{ ms}$ typical of current CaBER designs, we find that $\eta_{0,\text{min}} \sim 50 \text{ mPa s}$. In fact, CaBER has been used to create observable bridges for fluids with $\eta_0 \sim 11 \text{ mPa s}$ [12], but aqueous solutions of lower viscosities have not been studied. Thus,

$\eta_{0,\min} = 10 \text{ mPa s}$ represents a conservative estimate for the lower limit of operability of current designs of CaBER.

The use of SAW-induced microjets circumvents this problem by allowing the creation of liquid bridges within much smaller intervals δt_0 , while avoiding the problems induced by the mechanical separation of end-plates in conventional CaBER designs. A SAW is an electroacoustic wave that travels along the surface of a material, possessing an amplitude that decreases exponentially with depth in the medium. The use of SAWs to generate liquid jets from sessile droplets has been recently demonstrated [3] using a simple yet specific electrode configuration that acts to focus the energy of the electroelastic SAW (typically of 1–10 nm in amplitude). The SAW propagates along the substrate surface to a spot with a size equivalent to the wavelength of the acoustic radiation such that a part (determined by the relative acoustic impedance) of the concentrated energy ‘leaks’ into a droplet placed at the acoustic focal point. With sufficient acoustic wave intensity, acoustic streaming [13] results in the fluid, elongating the droplet perpendicular to the substrate and into a column of fluid—a jet—a few centimeters in length.

Over the following pages, the technique used to generate fluid bridges suitable for rheometry from Newtonian and non-Newtonian fluids possessing low viscosities is introduced. Results on the rheometry of water, polystyrene solutions and solvents follow, and are concluded by measurements of the rheology of dilute solutions of fibrinogen (FN) in water. We aim to show with these results that our system, described here for the first time, is capable of measuring the extensional rheology of low-viscosity fluids that are otherwise impossible to test using current technology.

2. Experiment

The SAW device used in these experiments is a variant of the device reported in [3] with a resonance frequency of 30 MHz. Details of the fabrication of the device are documented elsewhere [14, 15]. Briefly, the SAW was generated by supplying a sinusoidal voltage to an interdigital transducer (IDT) fabricated on a 0.5-mm-thick lithium niobate (LN) piezoelectric crystal. The section between the IDTs was coated with a thin layer of Teflon (Teflon AF, DuPont, Wilmington, Delaware, USA) in order to provide a hydrophobic surface. Single drops were placed with a pipette (Eppendorf PhysioCare Concept 0.1–2.5 μl , Hamburg, Germany) at the focal point of the IDTs before subjecting the fluid to a SAW burst, a controlled, intense exposure of the droplet to SAWs driven by a signal generator–amplifier combination. A photograph of the configuration with the quiescent droplet is shown in the left panel of figure 1(a). A 20 MHz waveform generator (33220A, Agilent, Santa Clara, CA, USA) was used to determine the burst time by triggering a second signal generator (WF1966, NF Corporation, Yokohama, Japan) over a fixed, predefined amount of time. The latter delivered a sinusoidal signal to an RF power amplifier (411LA, ENI, West Henrietta, NY, USA), providing a fixed frequency and amplitude signal near the resonance frequency of the SAW device. In order to obtain a liquid bridge, a glass plate was placed directly opposing the plate containing the SAW device as shown in the right panel of figure 1(a). Using this technique we have been able to create liquid bridges in 7.5 ms, about seven times quicker than existing technology, presenting us with the ability to observe the capillary-thinning behavior of fluids with viscosity of the order of 1 mPa s, much lower than $\eta_{0,\min}$.

An advantage of using SAWs for creating liquid bridges is that δt_0 , the time taken to create a bridge using a given fluid, can be reduced by increasing the voltage driving the IDTs.

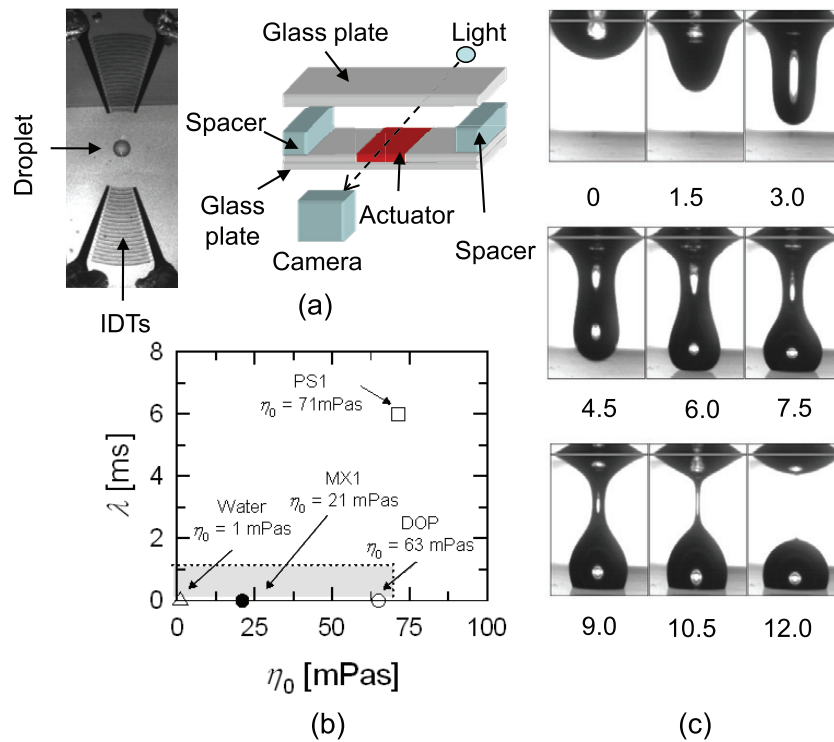


Figure 1. (a) Left panel: two focusing electrodes at the ends of an LN substrate are shown. The electrodes provide a focused SAW that progresses beneath and into the drop placed on the substrate at the focal point, causing it to deform into a coherent elongated jet. Right panel: schematic of the experimental setup for creating the liquid bridge. During experiments the setup is inverted so that the droplet jets downward and along the direction of gravity. (b) Solutions used in the study are indicated with respect to their viscosity and relaxation time in a manner similar to previous work [11]. The shaded region is difficult to access in conventional CaBER experiments due to limitations of current technology. (c) Using this system, a coherent jet forms from the droplet and subsequently becomes a liquid bridge as it reaches the opposite surface. The bridge necks down under the influence of capillary forces acting at the interface. The numbers correspond to the time in milliseconds. The gray line on the top refers to the surface of the plate containing the SAW actuator. For rheometric measurements the start time is $t_0 = 7.5$ ms, the time at which the SAW actuation is terminated for the shown experiment.

In figure 2, the decrease in time required to make a liquid bridge of DOP across two glass plates separated by 10 mm with increasing voltage is shown. The volume of test fluid required for use in the system is only about $1\text{--}5\ \mu\text{l}$, three orders of magnitude smaller than the volume required in current techniques.

The energy that leaks into the droplet is dependent on the size of the droplet relative to the aperture of the SAW IDT, the contact angle of the fluid, and the amplitude of the induced SAW in a complex, most nonlinear manner [16]. Further, as the viscosity is reduced, more accurate control of the separation distance and the alignment of the end-plates were found to be

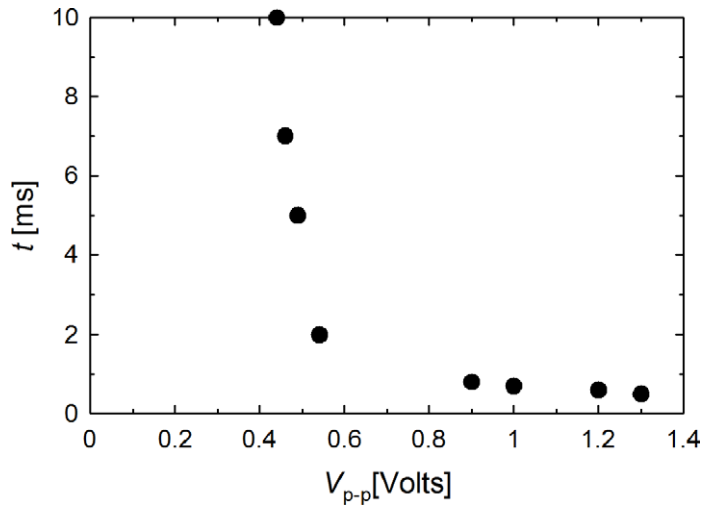


Figure 2. Voltage against time taken to create a liquid bridge of DOP from a $1 \mu\text{l}$ droplet. Plate separation is held constant at 10 mm. Note how the time taken to form a fluid bridge dramatically increases once the voltage falls below about 0.7 V.

necessary. The design described here allows only limited control of these variables. However, it was observed that careful control of the excitation voltage was sufficient to significantly enhance the reproducibility of the breakup time of liquid bridges (especially for water). Without due care in ejecting the droplet, the droplet either failed to jet or atomized—simply burst into droplets, which is indeed useful for other applications [14], [17]–[19]—in a complex manner illustrated by the non-dimensional relationship plotted as a map in figure 3.

The map was generated using several glycerol–water solutions of different viscosities. The basis for constructing the phase map is the idea that jetting occurs in sessile drops when they acquire sufficient momentum due to acoustic streaming driven by SAW irradiation. We define here a non-dimensional number that represents the ratio of SAW forcing imposed on the droplet to the resistance offered by surface tension to change in surface area,

$$\Pi = \frac{P/c_s}{\gamma R_d}, \quad (1)$$

where P is the power of SAW forcing, c_s is the speed of sound in the fluid and R_d is the original droplet radius. Lighthill's [20] analysis suggests that acoustic streaming can be expected when the ratio $\rho P/(c_s \eta_0^2) = \Pi/Oh^2$ exceeds a value of around 10, where

$$Oh = \frac{\tau_v}{\tau_R} = 14.1 \frac{\eta_0}{\sqrt{\rho \gamma R_d}} \quad (2)$$

measures the relative importance of viscous over inertial effects, the time-scale of the latter being quantified by the Rayleigh time, $\tau_R = \sqrt{\rho R_d^3/\gamma}$. Thus, on a plot of Π against Oh , we expect jetting in the region above the line $\Pi \approx 10 Oh^2$.

For any given Oh , we find that at relatively low non-dimensional values of the power, the droplet only slightly deforms from the surface as a 'stub'. As power input is increased, however, there is a transition to jetting (demarcated by + symbols). Although the expectation is that the transition from stubs to jetting should occur across a straight line of slope 2 on a log–log plot, the

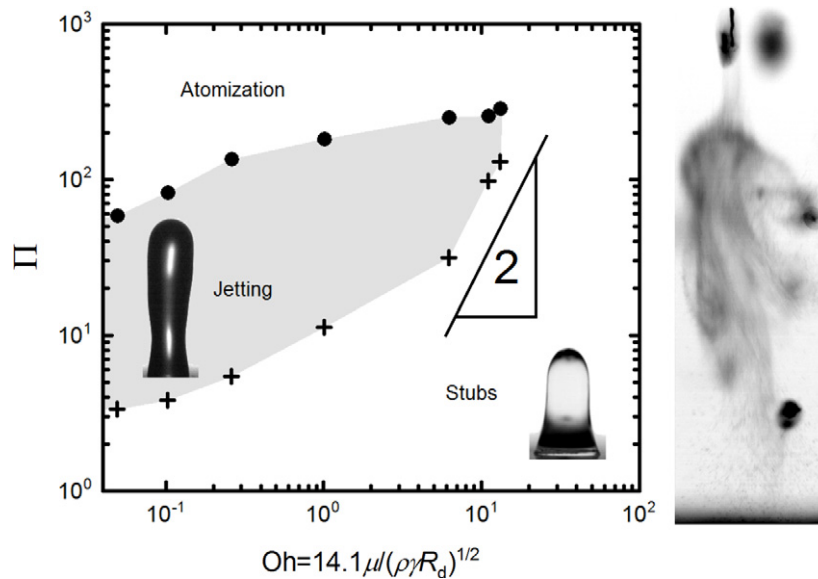


Figure 3. A map of the phenomena that can be generated by passing a SAW into a droplet sitting at the focal point atop the device shown in figure 1. Equations (1) and (2) in the text define the dimensionless numbers Π and the Ohnesorge number Oh . The photograph on the right shows typical behavior in the atomization regime at large values of Π .

transition line is actually slightly curved upwards in figure 3. We believe this is due to the effects of compressibility. Under most conditions in microfluidics, compressibility is negligible, but high-frequency acoustic waves induce significant density gradients, an important mechanism for acoustic streaming. The Ohnesorge number contains the density ρ in the denominator, and as the power is increased, the value of this density is left constant for the purposes of the plot, whereas in reality the actual density becomes larger as a consequence of the compression during exposure to the SAW [21]. The plotted Ohnesorge number is thus actually lower than it actually is in the experiment if we were to use the true value for the density. The problem is that the determination of the *correct* density value is very difficult.

At very high powers, we observe that jets atomize (demarcated by ● symbols and illustrated with the image to the right of the graph). Further, at large values of Oh we find that drops tend to atomize directly as power is increased without first forming jets. The phenomena that lead to atomization are currently not well understood. Nonetheless, the gray region represents the parameter space where SAWs can be used to create liquid bridges, and is thus useful for rheometry and rheology.

Following excitation of the droplet by SAWs and formation of the liquid bridge between the two plates, SAW excitation was turned off when a near-equal distribution of the material between the plates was obtained. As discussed above, SAW-induced jetting is the result of acoustic streaming. Therefore, once the liquid bridge is formed, we shut off SAW forcing to avoid any complications that may arise from a coupling between acoustic streaming and fluid rheology. The bridge then thins solely under the influence of surface tension, and we analyze the subsequent time evolution of R_{neck} as in the conventional CaBER device.

Images of the necking process were captured using a high-speed camera (Mikrotron MC1310, Germany) with a lens (InfiniVar CFM-2/S, Infinity Photo-Optical Company, Boulder,

Table 1. Physical properties of the fluids used in this study, organized by decreasing viscosity η_0 . PS1 is a 0.04% by weight solution of high-molecular-weight polystyrene ($M_w = 7.0$ MDa) in dioctyl phthalate (DOP) (Hopkin and Williams Ltd). MX1 is a 1 : 3 solution of DOP (Hopkin and Williams Ltd) and diethyl phthalate (DEP) (Aldrich Chemical Company, Inc.). The c/c^* ratio for the polystyrene solution is 0.887 and its Deborah number $De = \lambda/\tau_v$ is 0.198².

Fluid	γ (N m ⁻¹)	η_0 (Pa s)	τ_v (s)	τ_R (s)	Oh
PS1	3.0×10^{-2}	7.1×10^{-2}	1.0×10^{-1}	2.9×10^{-2}	3.4
DOP	3.0×10^{-2}	6.3×10^{-2}	8.9×10^{-2}	2.9×10^{-2}	3.0
MX1	3.2×10^{-2}	2.1×10^{-2}	2.8×10^{-2}	2.9×10^{-2}	0.92
Water	7.2×10^{-2}	1.0×10^{-3}	5.9×10^{-4}	1.9×10^{-2}	3.6×10^{-2}

²The diluteness of a polymer solution is characterized in terms of the ratio of the polymer concentration c over its critical value c^* at which polymeric coils begin to interpenetrate in solution. Both c^* and the time constant λ for the polymer solution, have been calculated using standard methods [38].

CO, USA) attachment. A single LED lamp was used to illuminate the liquid bridge in bright-field view (the bridge was placed between the lamp and the camera) and a 1.25 mm diameter wire was used as a visual reference during recording. Images were collected at 5000 frames per second and were analyzed using ImageJ (National Institutes of Health, Bethesda, MD, USA). The breakup event could be ascertained within ± 0.5 ms using this approach. An example of bridge formation and necking behavior is demonstrated in figure 1(c). It can be observed from figure 1(c) that the liquid bridge is formed at around 7.5 ms and breaks up at around 12 ms.

3. Results

3.1. Benchmark solutions

Details of the fluids studied with the technique discussed above are provided in table 1, where the viscous time, $\tau_v = 14.1\eta_0 R/\gamma$, and the Rayleigh time, $\tau_R = \sqrt{\rho R^3/\gamma}$, presume a length scale of $R = 3$ mm, a typical radius used in a CaBER experiment, and is used to facilitate comparison. Also listed in the table are the values of $Oh = \tau_v/\tau_R$. Strictly speaking, only fluids having $\tau_v \ll \tau_R$ can be considered to be low-viscosity fluids [11]. However, due to the restrictions imposed by the opening time (δt_0) this limit is seldom accessible in CaBER experiments. The present experiments are, thus, significant in this context. The range of CaBER is shown in figure 1(b), where the shaded region denotes the area where CaBER experiments are impractical due to the limitations of current technology. The diagram follows the one shown by Rodd *et al* [11], although in the present case the boundaries are marked by straight lines, instead of a curve, for simplicity. These limits can be marginally altered by a judicious choice of the geometry and operating conditions, but the differences are not remarkable. The points on the diagram in figure 1(b) identify the fluids used in this work.

In figure 4 the capillary-thinning behavior of Newtonian liquids used in this work is shown. The ratio of the minimum (instantaneous) radius ($R_{\text{neck}}(t)$) normalized by the initial radius of the liquid bridge (R_0) is plotted against time (t). On all occasions the minimum in the radius was observed to occur near the mid-point of the liquid bridge. Figure 4(a) presents our measurements for viscous samples for which $Oh \gtrsim 1$. We have also included data on glycerol from McKinley

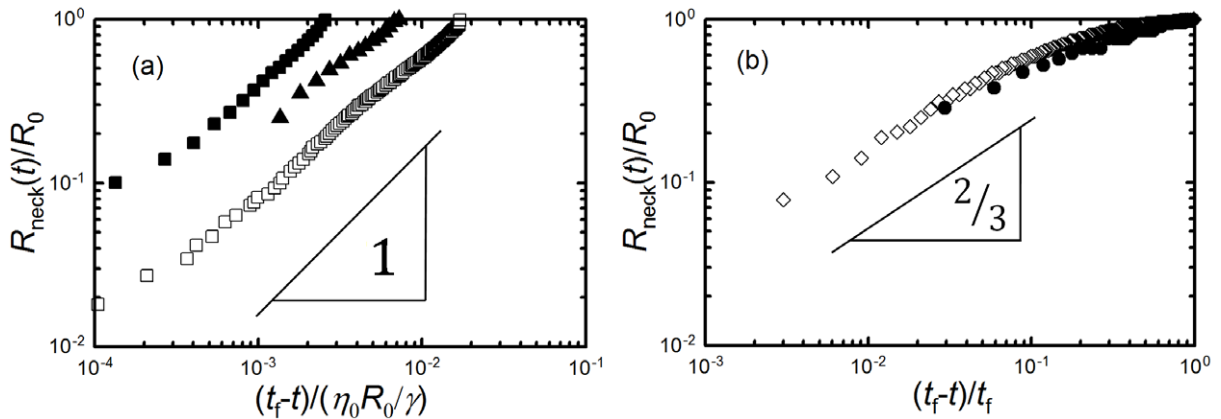


Figure 4. (a) Normalized minimum filament radii of bridges of viscous ($Oh \gtrsim 1$) fluid samples, namely, DOP (■) and MX1 (▲), plotted against time t expressed in terms of the normalized time to breakup, $(t_f - t)/t_f$, t_f being the breakup time observed in the experiments. Previous data using glycerol (□) by McKinley and Tripathi [22] are also included for comparison. Viscous Newtonian liquid bridges are expected to thin linearly with time close to breakup. (b) Data for inertia-dominated ($Oh \lesssim 1$) water liquid bridges using falling-drop (◇) and SAW (●) experiments, which are expected to thin such that $R(t_f - t)^{2/3}$ near breakup.

and Tripathi's work [22] for comparison. For viscous fluid threads undergoing surface tension-driven necking, it is expected that $R_{\text{neck}}(t) \sim (t_f - t)(\gamma/\eta_0)$, where t_f is the time at which the breakup event occurs, γ is the surface tension coefficient and η_0 is the zero-shear rate viscosity of the fluid [23]. The predicted linear trend is observed in the data in figure 4(a). It can also be seen that as the viscosity of a fluid decreases, breakup occurs earlier. For water, however, $Oh < 1$, and inertial effects become significant. In figure 4(b), we compare the data obtained on liquid bridges with the data obtained in falling-drop experiments by Amarouchene *et al* [9]. In this case, the observed decay approaches the asymptotic behavior $R_{\text{neck}} \sim (t_f - t)^{2/3}$ expected for thin filaments in the limit of vanishing viscosity [24].

The change in the capillary-thinning behavior due to the addition of a small quantity of long-chain polymer molecules is shown in figure 5(a). Here the response of the polystyrene solution PS1 is compared with that of the solvent, DOP. The neck radius for both viscous solutions initially decreases in a linear fashion with respect to time, although the rate of decrease for PS1 is slower due to its slightly higher viscosity from the dissolution of the polymer. Unlike DOP, which quickly undergoes breakup, PS1 abruptly transitions to a regime where $R_{\text{neck}}(t)$ decreases exponentially with time; the bridge narrows to a slightly smaller diameter but survives for approximately six times as long. In a capillary-thinning experiment involving a polymer solution, the elastic stresses can grow large enough to overwhelm the viscous stresses in the neck [2, 25, 26]. In fact, when the elasto-capillary stress balance dominates, the filament radius decays as $R_{\text{neck}}(t) \sim e^{-t/(3\lambda)}$, where λ is a characteristic relaxation time of the viscoelastic fluid [2, 11]. For polymer solutions, there is currently some debate concerning the interpretation of this relaxation time extracted from CaBER experiments and its relationship to the intrinsic relaxation time of polymer molecules [12, 27]. Nevertheless, this measured λ is a clear signature of polymer-induced elasticity.

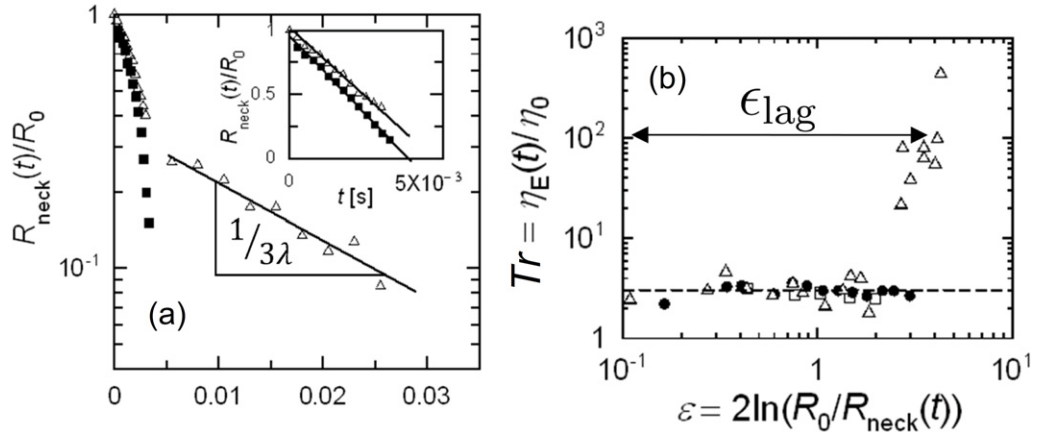


Figure 5. (a) Capillary-thinning behavior of a polymer solution PS1 (Δ) shows distinctly different behavior when compared to that of the solvent DOP (\blacksquare). While the radius of the DOP filament decreases linearly with time, the breakup process in PS1 is arrested, and a pronounced exponential-decay regime is observed, as indicated by the solid line corresponding to an exponential fit, producing a slope of $1/(3\lambda)$. Data corresponding to the first 5 ms are shown in the inset. It can be observed that the initial necking process progresses linearly with respect to time in both cases. (b) Transient Trouton ratio evaluated using equation (3) for the solutions PS1 (Δ), DOP (\bullet) and MX1 (\square) plotted against Hencky strain ε . Note that PS1, DOP, MX1 and water are in order of decreasing viscosity.

Based on an analysis by McKinley and Tripathy [22], the following semi-empirical relation was suggested by Tuladhar and Mackley [28] to fit filament-thinning data and extract the transient Trouton ratio Tr , which is defined as the ratio of the transient extensional viscosity to the zero-shear rate viscosity of the fluid:

$$Tr = \frac{\eta_E(t)}{\eta_0} = (2X - 1) \left[\frac{\gamma/\eta_0}{-2 dR_{neck}/dt} \right]. \quad (3)$$

For a Newtonian fluid, the extensional viscosity $\eta_E = 3\eta_0$, and hence $Tr = 3$, whereas for viscoelastic fluids such as polymer solutions, Tr is in general time dependent. The constant X is a lumped parameter that accounts for the combined effects of inertia, gravity and deviation of filament shape from a perfect cylinder. Theoretical analyses have shown that X ranges from 0.53 to 0.71 for Newtonian fluids, depending on whether inertial or viscous effects dominate. For polymer solutions, Tuladhar and Mackley used the equation to empirically fit X to ensure that $Tr = 3$ in the initial stages of filament thinning, when the contribution of the polymer to fluid stresses is negligible, and the fluid behaves as a viscous Newtonian fluid. Once the elastic stress induced by stretching polymer molecules becomes significant, Tr begins to increase above the initial Newtonian plateau. We use the same procedure to estimate the transient extensional viscosity from the data in figures 4(a) and 5(a), numerically calculating dR_{neck}/dt from the data with a three-point central-difference formula. The values of X for PS1, MX1 and DOP are between 0.53 and 0.71. In figure 5(b), we plot the transient Trouton ratio against the Hencky strain at the necking plane, $\varepsilon = -2\ln(R_{neck}/R_0)$, for the fluids listed in table 1. The dotted line in figure 5(b) corresponds to the constant value of $Tr = 3$ for any Newtonian fluid. It can be

observed from figure 5(b) that the Newtonian fluids DEP and MX1 show a constant value of $Tr = 3$ up until the resolution limit of our optical system was reached. For the polymer solution PS1, on the other hand, the value of Tr rapidly increases from a value of 3 to around 100 after a lag. It has been shown [29, 30] that polymer stresses in a dilute solution undergoing an extensional flow become significant after a Hencky strain of $\epsilon_{\text{lag}} = 0.5 \ln(N_K)$, where N_K is the number of Kuhn segments in the polymer. For the polymer in PS1, $N_K \sim 10^4$ and $\epsilon_{\text{lag}} \sim 4.5$. The data in figure 5(b) therefore indicate that typical benchmark behavior of viscoelastic fluids can be reproduced in these systems in a manner consistent with the literature, particularly with dilute polymer solutions in low-viscosity solvents, which are routinely used for polymer characterization. Although a detailed analysis is beyond the scope of this study, it is possible for instance to use ϵ_{lag} as a simple relative test of molecular weight across several samples.

It must be mentioned here that in both conventional CaBER and our experiments the exact deformation history during the creation of the liquid bridge is difficult to ascertain. The initial flow of the fluid in this ‘pre-strain’ time interval δt_0 is quite complex: the fluid jet is formed and then ejected to make contact with the top end-plate. In our experiments, drop volumes are typically $5 \mu\text{l}$, with initial diameters of 1.5–2 mm. The time interval $\delta t_{\text{ps}} < \delta t_0$ for the ejected jet to bridge the 3 mm gap between the fixed end-plates is $O(1)$ ms for all the fluids we have tested. An upper bound on the extensional strain may hence be estimated by assuming ideal extensional flow during this entire process, and a cylindrical drop shape that gives a pre-strain $\epsilon_{\text{ps}} = \ln(\ell_{\text{final}}/\ell_{\text{initial}}) \approx \ln(3/2) \lesssim 1$. The strain rate $\dot{\epsilon}_{\text{ps}} = \epsilon_{\text{ps}}/\delta t_{\text{ps}} \sim O(10^2) \text{ s}^{-1}$, which seems high. However, for the polymer solution (PS1) we have studied, the measured viscoelastic relaxation time $\lambda \sim O(10^{-2})$, which gives a Weissenberg number estimate $Wi_{\text{ps}} = \lambda \dot{\epsilon}_{\text{ps}} \sim O(1)$ for the pre-strain phase. For these typical values of Wi_{ps} and ϵ_{ps} , we do not expect any significant elastic stresses during bridge formation. Figure 5 further provides evidence for this: the initial necking of the PS1 liquid bridge is quite similar to that of the solvent DOP, showing that the initial deformation during liquid bridge formation does not cause polymers to stretch.

3.2. Fibrinogen

We now apply the SAW-induced microjets to observe the behavior of a multimeric blood protein, FN, in elongational flow. FN is a soluble plasma glycoprotein that plays an important role in hemostasis and cell adhesion [31]. Within the vasculature, vascular proteins such as FN encounter hydrodynamic deformation rates that can be of the order of 1000 s^{-1} or more [32]. These deformation rates are capable of bringing about large changes in conformation that become important in a number of mechano-chemical responses like clotting via platelet aggregation [33, 34].

In figure 6(a), the thinning behavior of a 0.25% solution of FN (F2629, Sigma, USA) in demineralized water is shown. The zero-shear rate viscosity of the solution is close to that of water and therefore extensional rheological studies of such solutions have not been possible in the past. It can be observed from figure 6(a) that the initial profile of the thinning jet is identical to that of water (control) and deviates from it at a later time. The surface tension coefficient of FN solutions has been measured to lie between 0.04 and 0.05 N m^{-1} [35, 36]. We thus estimate Oh for these solutions to be around 5×10^{-2} , whereas for water $Oh = 3.6 \times 10^{-2}$ (table 1). Therefore, despite changes in surface tension, the value of Oh for FN solutions is still much smaller than 1, and one would expect inertia-dominated thinning as observed for water. However, figure 6(a) shows that the thinning of the FN solution is substantially different from

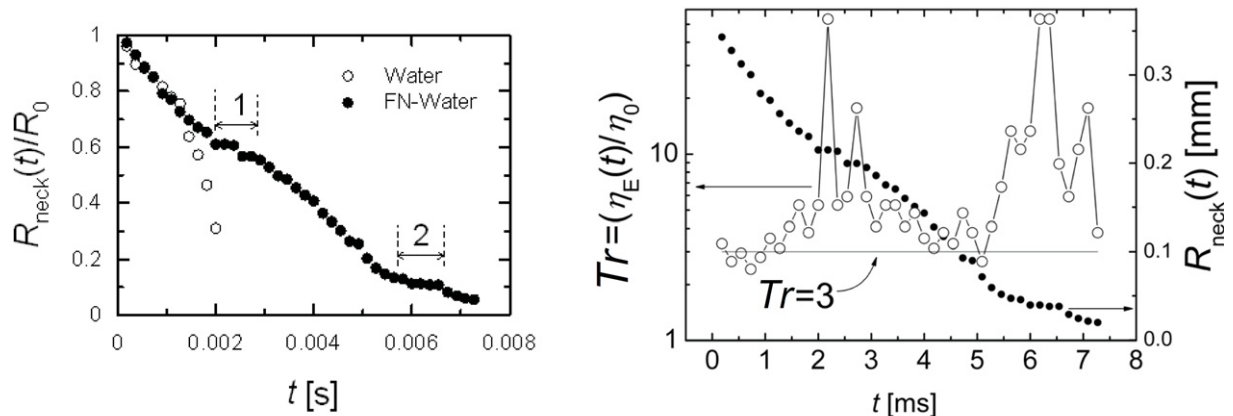


Figure 6. (a) Evolution of the normalized instantaneous diameter of 0.25% FN solution in demineralized water (○) compared with that of demineralized water alone (●). (b) Temporal evolution of the radius superposed on the calculated instantaneous Trouton ratio demonstrating the correspondence with each other. The horizontal line $Tr = 3$ is the value for a Newtonian fluid.

that of water. Further, the thinning rate for the FN solution substantially decreases (marked in figure 6(a) to facilitate identification) in between regions where the diameter shrinks steadily in time. At least two such regions can be identified in the present data.

As observed in figure 5(a) earlier, polymer-induced elastic stresses can resist the thinning of the filament, and it is possible that the two slowdowns in events in figure 6(a) are due to elastic stresses caused by the dissolved FN molecules. This is further highlighted in figure 6(b), where we plot the transient Trouton ratio calculated using equation (3) and the procedure described earlier (for the data in figure 6(b): $\gamma = 0.4 \text{ mN m}^{-1}$, $\eta_0 = 1 \text{ mPa s}$, $X = 0.51$). Although equation (3) is only strictly valid for viscous fluids when $Oh \gtrsim 1$, we use it as a qualitative tool to facilitate the discussion below. We have also retained the information on $R_{\text{neck}}(t)$ in figure 6(b) to emphasize that the maxima in the transient Trouton ratio correspond to regions where the rate of capillary thinning is dramatically reduced.

The complexity in the response in the FN solution probably arises from the multimeric structure of the molecule, in contrast to the simple backbone architecture of a homopolymer like polystyrene. It can be observed from figure 6(b) that as time (and the strain) increases, the transient Trouton ratio ascends above the Newtonian level of 3, and is over an order of magnitude above this value when the maxima are reached. At intermediate values of strain, however, the apparent Trouton ratio rapidly decreases, almost to the Newtonian level, and suggests that the stress accrued within the filament somehow relaxes. This is particularly interesting because the strain continues to increase during this time. With a further increase in strain, the transient Trouton ratio rises again and reaches approximately the same maximum level as previously corresponding to the second region of relatively slow reduction in $R_{\text{neck}}(t)$.

Single-molecule measurements using atomic-force microscopy have shown that compact domains in the secondary structure of proteins unfold under axial tension, and the force–displacement curves that result assume a sawtooth-like form that is characteristic of the protein studied [37]. The unfolding of protein domains typically manifests as sudden reductions among regular increases in the measured force with increasing elongation. It is tempting to speculate that the peaks in Tr in figure 6(b) are due to such stretch-and-yield events caused by

the rearrangements brought about by strong elongational flow. What is however demonstrably clear is that the behavior of low-viscosity biological fluids in extensional flows can now be studied using the apparatus described in this study. These types of fluids have been difficult to characterize due to their low viscosity (which impedes filament formation) and relatively restricted availability in large quantities (which prevents studies using large volumes of highly concentrated fluids). Both these impediments have been overcome by the application of SAWs in forming the fluid bridge.

4. Conclusions

In summary, we have demonstrated a method of using SAW-induced fluid jetting phenomena for extensional rheometry of low-viscosity Newtonian and non-Newtonian fluids. The technique thus opens up the possibility of measuring the elastic properties of low-viscosity fluids such as biological fluids and protein solutions. Understanding their viscoelasticity could complement other methods such as single-molecule force spectroscopy in the study of the molecular structure of complex macromolecules such as FN. Another application could be the development of an inexpensive portable microfluidic analytical kit to characterize viscoelastic samples, by combining the technique presented here with electrical resistivity or capacitance measurements to measure the neck radius.

Acknowledgment

We thank Dr D A Nguyen for his help with preparing and characterizing the fluids used in this study.

References

- [1] Keller A and Odell J A 1985 The extensibility of macromolecules in solution; a new focus for macromolecular science *Colloid Polym. Sci.* **263** 181–201
- [2] Anna S L and McKinley G H 2001 Elasto-capillary thinning and breakup of model elastic liquids *J. Rheol.* **45** 115
- [3] Tan M K, Friend J R and Yeo L Y 2009 Interfacial jetting phenomena induced by focused surface vibrations *Phys. Rev. Lett.* **103** 24501
- [4] Pumir A and Siggia E D 1992 Finite-time singularities in the axisymmetric three-dimension Euler equations *Phys. Rev. Lett.* **68** 1511–4
- [5] Grauer R, Marliani C and Germaschewski K 1998 Adaptive mesh refinement for singular solutions of the incompressible Euler equations *Phys. Rev. Lett.* **80** 4177–80
- [6] Eggers J 1993 Universal pinching of 3D axisymmetric free-surface flow *Phys. Rev. Lett.* **71** 3458–60
- [7] Eggers J 1997 Nonlinear dynamics and breakup of free-surface flows *Rev. Mod. Phys.* **69** 865–930
- [8] Christanti Y and Walker L M 2002 Effect of fluid relaxation time of dilute polymer solutions on jet breakup due to a forced disturbance *J. Rheol.* **46** 733
- [9] Amarouchene Y, Bonn D, Meunier J and Kellay H 2001 Inhibition of the finite-time singularity during droplet fission of a polymeric fluid *Phys. Rev. Lett.* **86** 3558–61
- [10] Cooper-White J J, Fagan J E, Tirtaatmadja V, Lester D R and Boger D V 2002 Drop formation dynamics of constant low-viscosity, elastic fluids *J. Non-Newton. Fluid Mech.* **106** 29–59
- [11] Rodd L E, Scott T P, Cooper-White J J and McKinley G H 2005 Capillary break-up rheometry of low-viscosity elastic fluids *Appl. Rheol.* **15** 12–27

- [12] Clasen C, Plog J P, Kulicke W M, Owens M, Macosko C, Scriven L E, Verani M and McKinley G H 2006 How dilute are dilute solutions in extensional flows? *J. Rheol.* **50** 849–81
- [13] Riley N 1998 Acoustic streaming *Theor. Comput. Fluid Dyn.* **10** 349–56
- [14] Qi A, Yeo L Y and Friend J R 2008 Interfacial destabilization and atomization driven by surface acoustic waves *Phys. Fluids* **20** 074103
- [15] Tan M K, Friend J R and Yeo L Y 2007 Microparticle collection and concentration via a miniature surface acoustic wave device *Lab Chip* **7** 618–25
- [16] McHale G, Banerjee M K, Newton M I and Krylov V V 1999 Surface acoustic wave resonances in the spreading of viscous fluids *Phys. Rev. B* **59** 8262–70
- [17] Qi A, Yeo L, Friend J and Ho J 2010 The extraction of liquid, protein molecules and yeast cells from paper through surface acoustic wave atomization *Lab Chip* **10** 470–6
- [18] Friend J, Yeo L, Arifin D and Mechler A 2008 Evaporative self-assembly assisted synthesis of polymeric nanoparticles by surface acoustic wave atomization *Nanotechnology* **19** 145301
- [19] Forde G, Friend J and Williamson T 2006 Straightforward biodegradable nanoparticle generation through MHz-order ultrasonic atomization *Appl. Phys. Lett.* **89** 064105
- [20] Lighthill J 1978 Acoustic streaming *J. Sound Vib.* **61** 391
- [21] Shutilov V A 1988 *Fundamental Physics of Ultrasound* (New York: Gordon and Breach)
- [22] McKinley G H and Tripathi A 2000 How to extract the Newtonian viscosity from capillary breakup measurements in a filament rheometer *J. Rheol.* **44** 653
- [23] Papageorgiou D T 1995 On the breakup of viscous liquid threads *Phys. Fluids* **7** 1529
- [24] Eggers J and Villermaux E 2008 Physics of liquid jets *Rep. Prog. Phys.* **71** 036601
- [25] Bazilevskii A V, Entov V M, Lerner M M and Rozhkov A N 1997 Failure of polymer solution filaments *Polym. Sci. A* **39** 316–24
- [26] Bazilevskii A V, Entov V M and Rozhkov A N 2001 Breakup of an Oldroyd liquid bridge as a method for testing the rheological properties of polymer solutions *Polym. Sci. A* **43** 716–26
- [27] Prabhakar R, Prakash J R and Sridhar T 2006 Effect of configuration-dependent intramolecular hydrodynamic interaction on elastocapillary thinning and breakup of filaments of dilute polymer solutions *J. Rheol.* **50** 925–47
- [28] Tuladhar T R and Mackley M R 2008 Filament stretching rheometry and break-up behaviour of low viscosity polymer solutions and inkjet fluids *J. Non-Newton. Fluid Mech.* **148** 97–108
- [29] Hinch E J 1994 Uncoiling a polymer molecule in a strong extensional flow *J. Non-Newton. Fluid Mech.* **54** 209–30
- [30] Prabhakar R, Prakash J R and Sridhar T 2004 A successive fine-graining scheme for predicting the rheological properties of dilute polymer solutions *J. Rheol.* **48** 1251–78
- [31] Doolittle R F 1984 Fibrinogen and fibrin *Annu. Rev. Biochem.* **53** 195–229
- [32] Kroll M H, Hellums J D, McIntire L V, Schafer A I and Moake J L 1996 Platelets and shear stress *Blood* **88** 1525
- [33] Schneider S W, Nuschele S, Wixforth A, Gorzelanny C, Alexander-Katz A, Netz R R and Schneider M F 2007 Shear-induced unfolding triggers adhesion of von Willebrand factor fibers *Proc. Natl Acad. Sci. USA* **104** 7899
- [34] Zhang X, Halvorsen K, Zhang C Z, Wong W P and Springer T A 2009 Mechanoenzymatic cleavage of the ultralarge vascular protein von Willebrand factor *Science* **324** 1330
- [35] Katona E, Neumann A W and Moscarello M A 1978 Forced unfolding of coiled-coils in fibrinogen by single-molecule AFM *Biochim. Biophys. Acta* **534** 275
- [36] Hernández E M and Franses E I 2003 Adsorption and surface tension of fibrinogen at the air/water interface *Colloids Surf. A* **214** 249
- [37] Brown A E X, Litvinov R I, Discher D E and Weisel J W 2007 Forced unfolding of coiled-coils in fibrinogen by single-molecule AFM *Biophys. J.* **92** L39–41
- [38] Gupta R K, Nguyen D A and Sridhar T 2000 Extensional viscosity of dilute polystyrene solutions: effect of concentration and molecular weight *Phys. Fluids* **12** 1296